Available online at www.sciencedirect.com
SCIENCE DIRECT®
Journal of Photochemistry and Photobiology A: Chemistry 168 (2004) 67–73
Journal of Photochemistry and Photobiology A:Chemistry
www.elsevier.com/locate/jphotochem

# Photosensitisation and photoinduced DNA cleavage by four naturally occurring anthraquinones

M. Rajendran [a], R. Gandhidasan [b], R. Murugesan [b,*]

[a] *Department of Chemistry, NMSSVN College, Madurai 625019, Tamilnadu, India*
[b] *School of Chemistry, Madurai Kamaraj University, Madurai 625021, Tamilnadu, India*

Received 28 September 2003; received in revised form 20 January 2004; accepted 13 February 2004
Available online 3 July 2004

**Abstract**

Photosensitising properties of four naturally occurring anthraquinones, viz., erythroglaucin (ERG), teloschistin (TEL), 1-hydroxy-2-methylanthraquinone (HYQ) and 1-methoxy-2-hydroxyanthraquinone (MEQ) are studied. Photogeneration of singlet oxygen was monitored by both optical RNO (*para*-nitrosodimethylaniline) bleaching and electron paramagnetic resonance spectroscopy (EPR)-2,2,6,6-tetramethyl piperidinol (TEMPL) methods. In comparison with rose bengal (RB), singlet oxygen generating efficiencies of ERG, TEL, HYQ and MEQ are determined to be 0.10, 0.14, 0.02 and 0.13, respectively. The formation of $O_2^{\bullet -}$ was monitored by optical spectroscopy using SOD inhibitable cytochrome *c* reduction assay. Photolysis of ERG and MEQ in DMSO, in the presence of 5,5-dimethyl-1-pyrroline-*N*-oxide (DMPO) generated a multiline EPR spectrum characteristic of mixture of $O_2^{\bullet -}$, $^{\bullet}OH$ and $^{\bullet}OCH_3$ adducts. Both electron transfer (Type I) and energy transfer (Type II) paths are involved in the photosensitisation of ERG, TEL, HYQ and MEQ. Quantum efficiencies of the quinones exhibit correlation with their half-wave potentials. The photoinduced DNA cleavage by quinones was examined with covalently closed circular plasmid DNA, in vitro. Observed DNA photo strand scission correlates with the reactive oxygen species (ROS) generating efficiencies of the quinones.


*Keywords:* Anthraquinones; Photosensitisation; Singlet oxygen; Superoxide anion; Spin trapping; DNA strand break; EPR

## 1. Introduction

Quinones are widely distributed in nature and are used clinically for the treatment of a wide variety of malignancies [1]. Anthracycline derivatives constitute an important class of anticancer drug [2]. Many such anthraquinone derivatives possess the ability to mediate one electron transfer to molecular oxygen to form superoxide anion radical and to generate reactive oxygen species (ROS) upon visible light illumination. The photodynamic generation of superoxide anion radicals by doxorubicin and daunorubicin has been demonstrated [3]. Aminoanthraquinone derivatives are also shown to photosensitise human leukemic cells in culture [4]. We have undertaken a systematic investigation of photodynamic action of various natural as well as synthetic quinones [5,6]. In our earlier studies we have investigated the photodynamic action and cytotoxic effect of various quinones such as barleriaquinone-I, barleriaquinone-II, mansonone-D, mansonone-H, thespone and thespesone [7,8]. Photoexcited quinones can produce ROS via two pathways. Absorption of light excites photosensitisers from ground state (S) to a triplet excited state ($^3$S). In Type I reactions, $^3$S participates in electron transfer or hydrogen abstraction reactions with nearby molecules, followed by fast addition of oxygen to form peroxyl radicals. In Type II reactions, $^3$S can transfer its excitation energy to $O_2$ to form nonradical singlet oxygen.

In the present study, we have investigated the mechanism of photogeneration of ROS by four anthraquinone derivatives, ERG, TEL, HYQ and MEQ. In addition, photoinduced plasmid DNA strands break by these quinones is also investigated.

## 2. Materials and methods

### 2.1. Chemicals

Superoxide dismutase (SOD), catalase and cytochrome *c* were purchased from Sigma Chemical Co., while reduced nicotinamide adenine dinucleotide (NADH) was obtained from Boehringer Mannheim. Dimethyl sulphoxide

* Corresponding author. Tel.: +91-452-2458471; fax: +91-452-2459105.
*E-mail address:* rammurugesan@yahoo.com (R. Murugesan).

1010-6030/$ – see front matter © 2004 Elsevier B.V. All rights reserved.
doi:10.1016/j.jphotochem.2004.02.014

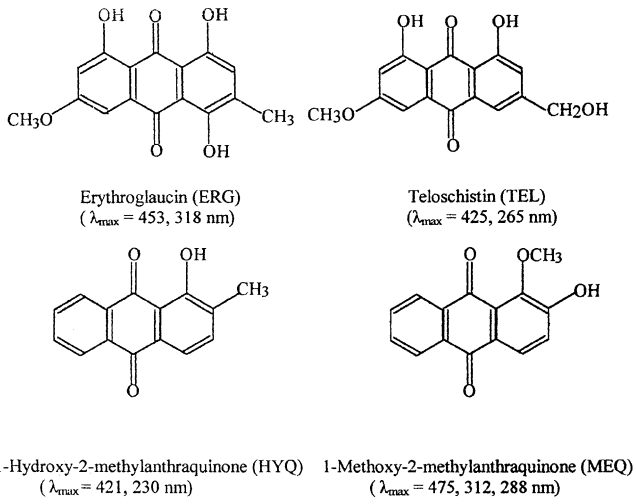


Fig. 1. Chemical structures of ERG, TEL, HYQ and MEQ.

(HPLC grade) was purchased from Qualigens Fine Chemicals. *N*,*N*-Dimethyl-4-nitrosoaniline (RNO), 1,4-diazabicyclo[2,2,2]octane (DABCO), diethyltriaminopentaacetic acid (DETAPAC) and rose bengal (RB) were obtained from Aldrich. The spin trap 5,5-dimethyl-1-pyrroline-*N*-oxide (DMPO) was obtained from Aldrich and was purified by activated charcoal [9]. 2,2,6,6-Tetramethyl piperidinol (TEMPL) was obtained from Merck. Imidazole, ethylenediaminetetraacetic acid (EDTA) and sodium azide were purchased from S.D. Fine Chemicals (India). Imidazole was used after repeated crystallisation from doubly distilled water. All other compounds were used as received.

The chemical structures of the quinones studied are given in Fig. 1. These quinones were received as gift from the Department of Natural Products Chemistry, Madurai Kamaraj University, Tamilnadu, India. The purity of the compounds was checked by recording the $^1$H NMR spectra on a BRUKER 300 spectrometer with tetramethylsilane as an internal standard and ($(CD_3)_2SO$) as solvent. NMR spectral data (chemical shift in $\delta$, ppm) for ERG: 13.31 (s, 1H, 8-OH), 12.80 (s, 1H, OH), 12.32 (s, 1H, OH), 7.37 (d, 1H, 5-H), 7.21 (s br, 1H, 2-H), 6.79 (d, 1H, 7-H), 3.97 (s, 3H, $OCH_3$), 2.58 (d, 3H, 3-$CH_3$). NMR spectral data for HYQ: 12.9 (s, 1H, 1-OH), 8.21–8.29 (m, 2H, 5,8-H), 8.09 (s, 1H, 4-H), 7.82–7.95 (m, 2H, 6,7-H), 7.67 (s br, 1H, 3-H), 2.35 (s, 3H, 2-$CH_3$). NMR spectral data for TEL: 12.0 (s, 2H, 1,8-OH), 7.63 (s, 1H, 4-H), 7.26 (d, 1H, 5-H), 7.13 (s, 1H, 2-H), 6.78 (d, 1H, 7-H), 4.67 (s br, 2H, 3-$CH_2O$), 3.95 (s, 3H, 6-$OCH_3$), 2.57 (s br, 1H, 3-OH). NMR spectral data for MEQ: 9.71 (s, 1H, 2-OH), 8.20 (m, 2H, 5,8-H), 7.99 (d, 1H, 4-H), 7.79 (m, 2H, 6,7-H), 7.32 (d, 1H, 3-H), 3.95 (s, 3H, 1-$OCH_3$).

### 2.2. Light source

Light source used for irradiation was a 150 W xenon lamp. A filter combination of 10 cm potassium iodide solution (1 g in 100 ml) and 1 cm pyridine was used to cut-off below 300 nm and to achieve a band-pass spectral window of 300–700 nm. The irradiation was carried out in an open cuvette in equilibrium with the atmosphere. The reaction mixture in a quartz cuvette placed at a distance of 12 cm from the light source was continuously stirred during irradiation.

### 2.3. Singlet oxygen assay

Singlet oxygen was detected by the method developed by Kraljic and El Mohsni [10]. The sensitiser was exposed to light in the presence of imidazole (10 mM) and RNO (50 mM) in a 50 mM phosphate buffer (pH 7.4). The bleaching of RNO was monitored spectrophotometrically at 440 nm, as a function of irradiation time. $^1O_2$ generated by photoexcitation of the quinone reacts with imidazole to form a transannular peroxide which bleaches RNO and the bleaching can be monitored spectrophotometrically. The intermediacy of $^1O_2$ in bleaching RNO is further confirmed by carrying out the reaction in the presence of scavengers specific to $^1O_2$ and following the inhibition of RNO bleaching. Shimadzu UV-Vis spectrometer (UV-160) as well as Specord S100 UV-Vis spectrometer (Analytik Jena AG, Jena, Germany) were used for optical measurements. The interference of $O_2^{\bullet-}$ and $H_2O_2$ on RNO bleaching was removed by the addition of SOD and catalase, respectively.

The rate of disappearance of quencher ($A$) obeys the following equation [11]:

$$-\frac{d[A]}{dt} = (I_{ab}\Phi^1O_2)\frac{K_r[A]}{K_d}$$

where $K_r$ is the rate constant for chemical quenching, $K_d$ the rate constant for deactivation of $^1O_2$ by the solvent and $I_{ab}$ the intensity of light absorbed by the sensitiser. The slope of the first-order plot is $I_{ab}\Phi^1O_2(K_r/K_d)$. The slope was calculated by curve fitting the experimental data [12]. Under similar conditions, experiments were carried with reference singlet oxygen generator, RB. The relative rate of slopes were corrected for molar absorption and photon energy [13]. The quantum yield of $^1O_2$ generation was determined for the sensitisers ERG, TEL, HYQ and MEQ using $\Phi^1O_2 = 0.76$ for RB [14]. The optical RNO bleaching method suffers a setback when the quinones and RNO absorb in the same region. Hence, in our studies the EPR-TEMPL method was also used to measure the $^1O_2$ yield.

In EPR technique the problems related to optical study are eliminated. The conversion of EPR silent TEMPL (2,2,6,6-tetramethyl piperidinol) to an EPR-detectable nitroxide-free radical TEMPOL (4-hydroxy-2,2,6,6-tetramethyl piperidine-1-oxyl) by the singlet oxygen can be readily monitored [15,16]. The quinone concentrations were adjusted so that the absorbances of photosensitised systems at absorption maxima were equal. Reaction mixture (1 ml) containing 0.01 M TEMPL and quinone in DMSO was irradiated. The irradiated samples were injected into

gas-permeable Teflon capillary tube (0.8 mm inside diameter, 0.5 mm wall thickness) which was folded and inserted into a narrow quartz tube and placed in the EPR cavity for measurements. The increase of EPR signal intensity was recorded at different times of irradiation.

### 2.4. Superoxide anion assay

Photogeneration of $O_2^{\bullet -}$ was detected by using SOD inhibitable cytochrome *c* reduction method [17]. Photosensitisers were illuminated in the presence of ferricytochrome *c* (40 μM) in 50 mM phosphate buffer (pH 7.4) in air atmosphere. The increase in absorbance was monitored spectrophotometrically at 550 nm, using $\Delta\epsilon_{550} = 20{,}000\ M^{-1}\ cm^{-1}$ for the reduced-oxidised cytochrome *c* [18].

EPR spin trapping experiments were also used to detect the generation of $O_2^{\bullet -}$ on photoirradiation of ERG and TEL. EPR spectra were recorded using JEOL JES-100 EPR spectrometer operating at X-band frequency with 100 kHz field modulation. The irradiated reaction mixture (1 ml), containing DMPO (100 mM) and quinone (200 μM) in DMSO, was drawn into gas-permeable Teflon capillary tubes (0.8 mm inside diameter, 0.5 mm wall thickness). Each capillary was folded twice, inserted into narrow quartz tube open at both ends and then placed in the EPR cavity. Experiments were repeated to monitor the signal intensity at different intervals of irradiation time. A BASIC computer program was used to simulate the EPR spectra.

### 2.5. Cyclic voltammetry

Redox potentials of acetonitrile solutions of quinones (2 mg; 5 ml acetonitrile) were investigated by using electrochemical analyser BAS 50A (Bioanalytical Systems, West Lafayette, IN). The electrochemical cell consists of a three electrode assembly of glassy carbon (working), platinum (auxiliary) and Ag/AgCl (reference) electrodes. Glassy carbon was resurfaced with alumina before use. Tetrabutylammonium perchlorate (TBAP) (50 mM) was used as a supporting electrolyte. Solutions were deoxygenated for 10 min with nitrogen gas prior to measurement and cyclic voltammograms were recorded under nitrogen atmosphere.

### 2.6. Photocleavage of DNA by quinones

Covalently closed circular (ccc) pUC19 plasmid DNA was prepared and purified by the method of Maniatis et al. [19]. The air-saturated solution containing DNA (3 μg) and quinone (1–2 mM) in phosphate buffer (pH 7.4) were irradiated in a gas-permeable Teflon tube. After the irradiation was over, 20 μl aliquot of the mixture was loaded into agarose gels (0.7%) in Tris–acetate–EDTA buffer, containing 0.05 μg/ml ethidium bromide. The electrophoresis was carried out for 1 h at 50 V. After electrophoresis, the gels were illuminated with UV light and photographed.

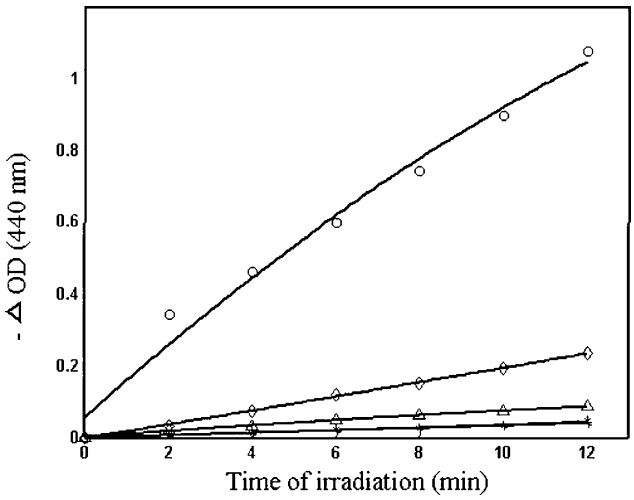


Fig. 2. Photosensitised RNO bleaching measured at 440 nm in the presence of imidazole (10 mM) in 50 mM phosphate buffer (pH 7.4) with RB (○), MEQ (◇), TEL (△), HYQ (∗) and ERG (×) as a function of irradiation time.

## 3. Results and discussion

### 3.1. Energy transfer process

Generation of $^1O_2$ was measured by RNO bleaching assay. The loss of RNO absorbance at 440 nm as a function of irradiation time for ERG, TEL, HYQ, MEQ and RB is shown in Fig. 2. Singlet oxygen generated by photoexcitation of the quinone reacts with imidazole to form transannular peroxide which bleaches the RNO [20]. The bleaching rate is used for calculating $^1O_2$ yield. The ratio of the slopes of RB to each quinone was corrected for molar absorption and photon energy to obtain the singlet oxygen generating efficiency of the quinones. The quantum yields thus evaluated are 0.10, 0.14, 0.02 and 0.13 for ERG, TEL, HYQ and MEQ, respectively.

To confirm the role of $^1O_2$ in bleaching of RNO, experiments were carried out in the presence of specific singlet oxygen quenchers such as DABCO and sodium azide. Fig. 3 shows the loss of RNO absorbance by MEQ in the presence of DABCO and azide. The singlet oxygen quenching rate constant of imidazole ($2 \times 10^7\ M^{-1}\ s^{-1}$) and DABCO ($1.5 \times 10^7\ M^{-1}\ s^{-1}$) are comparable [21]. In the presence of equal concentrations of imidazole and DABCO, it is expected that the quenching rate constant would be reduced by 50%. In this experiment, the measurements were carried out in the presence of 10 mM imidazole and 5 mM DABCO, hence the reduction rate constant was decreased by about 25%. Similarly sodium azide reacts with $^1O_2$ about 100 times faster than imidazole. But in the present study, the concentrations of sodium azide and imidazole used are 0.1 and 10 mM, respectively. Hence, at these concentrations, it was found that the RNO bleaching rate was inhibited by 50%. These results confirm the generation of $^1O_2$ during photodynamic process.

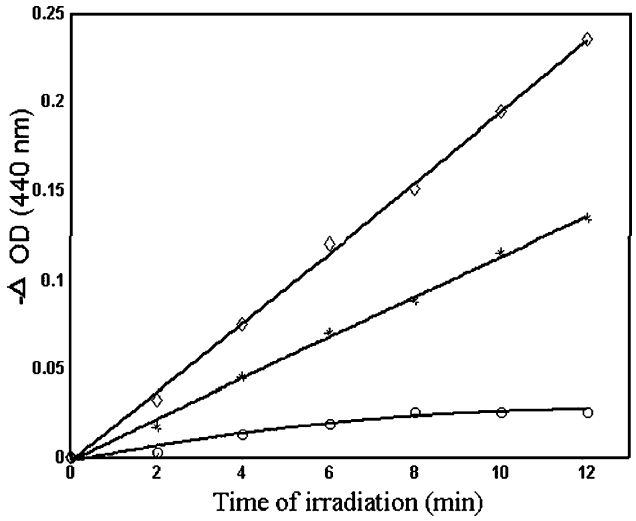


Fig. 3. Photosensitised RNO bleaching measured at 440 nm in the presence of imidazole (10 mM) in 50 mM phosphate buffer (pH 7.4) with MEQ (◇) as a function of illumination time in minutes. Inhibition of photosensitised RNO bleaching by MEQ in the presence of 0.1 mM sodium azide (○) and in the presence of 5 mM DABCO (∗).

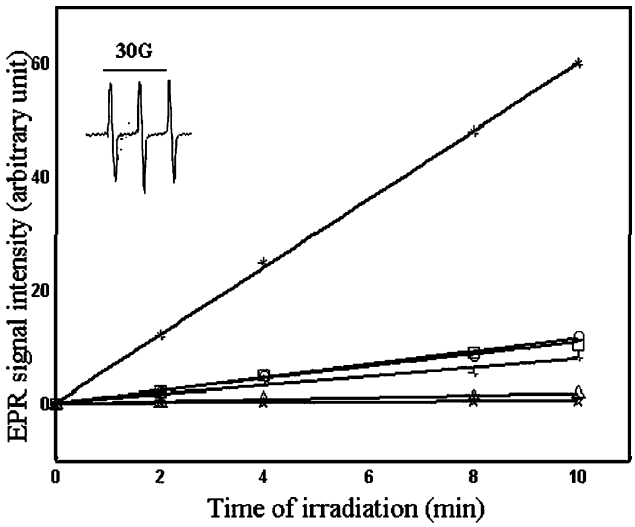


Fig. 4. The formation of TEMPOL during the photoirradiation of solutions containing RB (∗), TEL (○), MEQ (□), ERG (×), HYQ (△), in the presence of TEMPL (20 mM) at 300 K in DMSO. Inhibitory effect of 1 mM sodium azide (☆) on the intensity of TEMPOL radical during photoirradiation of MEQ. The inset shows the EPR spectrum of TEMPOL generated during the photoirradiation of DMSO solution of ERG in the presence of TEMPL. Spectrometer settings—microwave power: 2 mW; modulation amplitude: 1 G; time constant: 0.1 s; scans rate: 4 min.

EPR-TEMPL method was also used to detect the photogeneration of $^1O_2$ by ERG, TEL, HEQ and MEQ. When aerated solution of anthraquinones and TEMPL in DMSO was irradiated at room temperature, an EPR spectrum consisting of three equally intense lines characteristic of a nitroxide radical [TEMPOL] was detected. The hyperfine splitting constant ($A_N = 15.6$ G) was found to be identical with those of the authentic commercially obtained TEMPOL. EPR signal intensity of TEMPOL produced was found to increase with increase of irradiation time as shown in Fig. 4. No EPR spectrum was observed without sensitisers indicating that the formation of the nitroxide radical is a photodynamic process.

The generation of $^1O_2$ during the photoirradiation was further confirmed by studying the effect of sodium azide (Fig. 4) on the intensity of the EPR signal by using MEQ as a sensitiser. The generation of TEMPOL by anthraquinones was found to be parallel to their $^1O_2$ quantum yield estimated by RNO bleaching method. In EPR measurement (Fig. 4) the quinones concentrations were adjusted so that absorbances of quinones systems were equal. Hence absorbance corrections for EPR measurements were not necessary. From Fig. 4, the $^1O_2$ generating efficiency of RB, ERG, TEL, HYQ and MEQ were determined to be 1, 0.13, 0.19, 0.03 and 0.18, respectively, consistent with the values determined by the RNO bleaching method.

### 3.2. Electron transfer process

Generation of $O_2^{\bullet -}$ anion radical was detected by SOD inhibitable cytochrome *c* reduction assay. Fig. 5 shows the rate of cytochrome *c* reduction when air-saturated solutions of quinones were photolysed in the presence of EDTA, cytochrome *c* (40 μM) in phosphate buffer (pH 7.4). ERG, TEL, HYQ and MEQ were found to enhance the rate of cytochrome *c* reduction with different efficiencies. In the presence of electron donor EDTA the rate of cytochrome *c* reduction was enhanced (Fig. 5). As shown in Scheme 1, an electron donor D that can interact with the triplet state of a sensitiser can effectively switch the pathways from $^1O_2$ production into the generation of the $S^{\bullet -}$ species. Depending on the conditions, $S^{\bullet -}$ can interact with molecular oxygen to yield $O_2^{\bullet -}$, or directly react with a substrate via radical reactions, or enter into a redox reaction with an appropriate

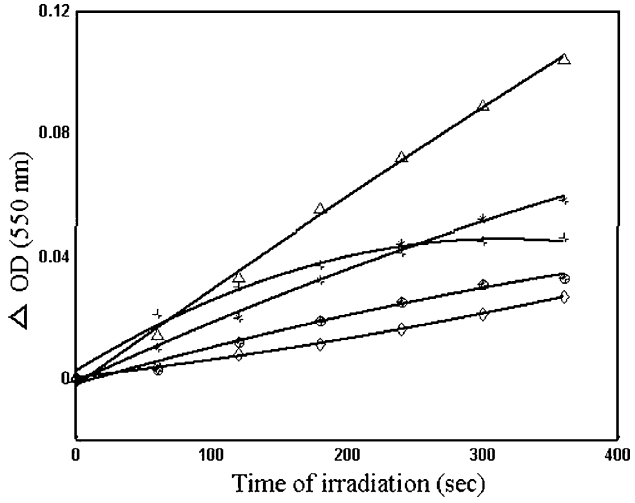


Fig. 5. Photosensitised cytochrome *c* reduction in the presence of EDTA by TEL (×), ERG (∗), HYQ (⊙), MEQ (△) and MEQ in the absence of EDTA (◇) as a function of irradiation time.

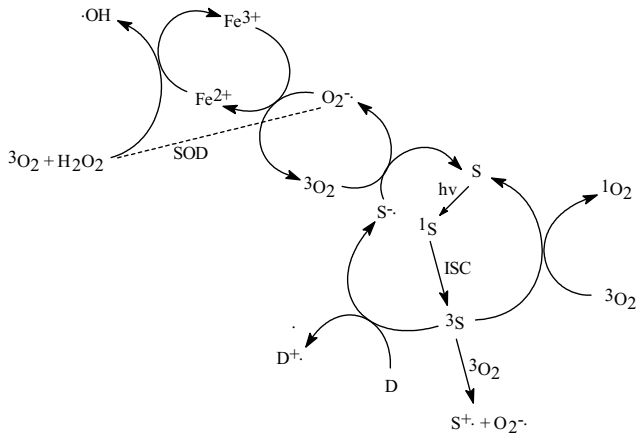


Scheme 1.

and available metal ion. The rates of superoxide generation in the presence of EDTA by ERG, TEL, HYQ and MEQ were determined to be 0.01, 0.015, 0.005 and 0.015 μM/s, respectively. The rates of $O_2^{\bullet -}$ generation efficiency in the absence of EDTA by ERG, TEL, HYQ and MEQ was found to be 0.0016, 0.0023, 0.0009 and 0.0025 μM/s, respectively. The $O_2^{\bullet -}$ generation efficiency enhancement in the presence of EDTA by MEQ is shown in Fig. 5.

The photogenerated $O_2^{\bullet -}$ from ERG was studied by EPR spin trapping experiment using DMPO as the spin trap. No EPR signal was observed either in dark (Fig. 6A) or when DMPO alone was irradiated in DMSO. However, a multiline EPR spectrum was observed when ERG (200 μM) was photolysed in the presence of DMPO (100 mM) in an air-saturated DMSO solution (Fig. 6B). In an aprotic solvent such as DMSO, DMPO-OOH adduct has longer life time [22]. The intensity of the EPR signal increased with increase of irradiation time. The observed EPR spectrum could be readily analysed in terms of a mixture of three types of spin adducts. Hyperfine coupling constant (hfcc) values for one of the spin adducts was simulated as a primary nitrogen triplet ($A_N = 13.0$ G) split by a proton ($A_H^\beta = 10.7$ G) which is further split by a secondary proton ($A_H^\gamma = 1.25$ G). Hyperfine coupling constants for the second spin adduct are $A_N = 14.3$ G and $A_H^\beta = 11.8$ G and for the third spin adduct, the hfccs are $A_N = 13.3$ G, $A_H^\beta = 9.0$ G and $A_H^\gamma = 1.8$ G. These hfcc values are in good agreement with the reported values for DMPO-$O_2^{\bullet -}$, DMPO-OH and DMPO-$OCH_3$ [23–26]. EPR spectra of these three spin adducts were computer-simulated separately using the corresponding hfcc values. When these three spectra were combined in the ratio of 7:1.7:1.3 for $O_2^{\bullet -}$, $^\bullet$OH and $^\bullet OCH_3$, respectively, the simulated EPR spectrum (Fig. 6C) matched well with the experimentally observed one.

Addition of SOD (50 μg/ml) prior to irradiation inhibited the formation of the adduct (Fig. 6D), confirming the generation of $O_2^{\bullet -}$. Hydroxyl radical may be generated either from the decomposition of DMPO-OOH adduct or may directly be produced from the photoirradiation of the quinones. After addition of excess ethanol, DMPO-OH signal was not abolished, indicating that hydroxyl radical is not generated directly [27]. Hence the DMPO-OH signal was observed due to the decomposition of DMPO-OOH adduct only. The methyl radical may have its origin in the reaction between $^\bullet$OH and DMSO [28]. Control experiments confirm that ERG, oxygen and light are all necessary to produce DMPO adduct. Whereas under deoxygenated conditions, the methyl radical adduct was detected.

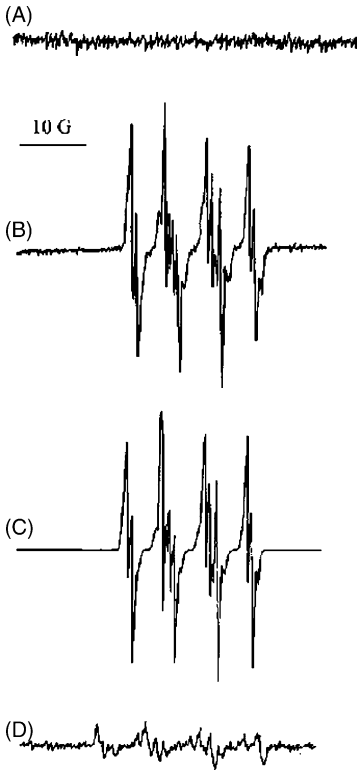


Fig. 6. EPR spectrum generated by irradiation of ERG (200 μM) and DMPO (100 mM) in air-saturated DMSO solution: (A) in the dark; (B) after 4 min irradiation. The spectrum contains three spin adducts: DMPO-$O_2^{\bullet -}$ ($A_N = 13.0$ G, $A_H^\beta = 10.7$ G, $A_H^\gamma = 1.25$ G); DMPO-OH ($A_N = 14.3$ G and $A_H^\beta = 11.8$ G); DMPO-$OCH_3$ ($A_N = 13.3$ G, $A_H^\beta = 9.0$ G, $A_H^\gamma = 1.8$ G) in the ratio of 7:1.7:1.3. (C) Computer-simulated spectrum obtained by summation of three spin adducts (see text). (D) After 4 min irradiation in the presence of SOD (50 μg/ml). Spectrometer settings—microwave power: 2.0 mW; modulation frequency: 100 kHz; modulation amplitude: 0.5 G; time constant: 0.1 s; scan rate: 4 min; receiver gain: 250.

DMPO spin trapping experiment was also carried out for MEQ as similar to that of ERG. The observed EPR spectrum could be readily analysed in terms of a mixture of two types of spin adducts. Hyperfine coupling constant values for one of the spin adducts was arrived as $A_N = 12.85$ G, $A_H^\beta = 10.4$ G and $A_H^\gamma = 1.3$ G. The hfccs of the other spin adduct are $A_N = 13.4$ G, $A_H^\beta = 8.5$ G and $A_H^\gamma = 1.3$ G. These spectra could be readily assigned to DMPO-$O_2^{\bullet -}$ and DMPO-$OCH_3$ respectively on the basis of reported hfcc val-

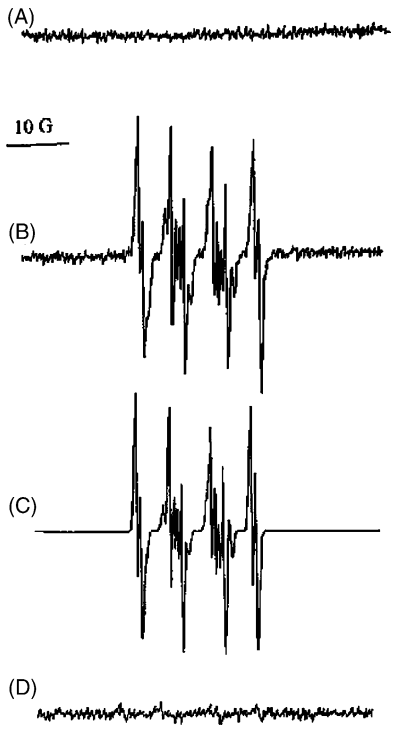


Fig. 7. EPR spectrum generated by irradiation of MEQ (200 μM) and DMPO (100 mM) in air-saturated DMSO solution: (A) in the dark; (B) after 4 min irradiation. The spectrum contains two spin adducts: DMPO-$O_2^{\bullet-}$ ($A_N = 12.8$ G, $A_H^{\beta} = 10.4$ G, $A_H^{\gamma} = 1.3$ G) and DMPO-$OCH_3$ ($A_N = 13.4$ G, $A_H^{\beta} = 8.5$ G, $A_H^{\gamma} = 1.8$ G) in the ratio of 8.2:1.8. (C) Computer-simulated spectrum obtained by summation of two spin adducts. (D) After 4 min irradiation in the presence of SOD (50 μg/ml). Spectrometer settings—microwave power: 2.0 mW; modulation frequency: 100 kHz; modulation amplitude: 0.5 G; time constant: 0.1 s; scan rate: 4 min; receiver gain: 500.

ues [23–26]. When the two spectra were added up in the ratio of 8.2:1.8 for $O_2^{\bullet-}$ and $^{\bullet}OCH_3$ respectively, the simulated EPR spectrum (Fig. 7C) matched well with the experimentally observed one. Addition of SOD prior to illumination prevents the formation of spin adduct as shown in Fig. 7D as observed in the case of ERG.

### 3.3. Redox potentials

The electrochemical parameter frequently used in structure–activity relationship study is the half-wave potential of the quinone reduction [29]. Hence an attempt was made to correlate the structure of quinone and half-wave potential. Well-defined cathodic and anodic peaks were observed in the cyclic voltammogram of the compounds. The electrochemical data for ERG, TEL, HYQ and MEQ are given in Table 1. The observed first wave $E_{1/2}$ is in the order TEL > MEQ > ERG > HYQ, which matches with the $O_2^{\bullet-}$ generating efficiency of the quinones [30]. The relationship between photogenerated $O_2^{\bullet-}$ and the reduction potential of quinone is due to the possibility of involvement of Type I reaction in preference to Type II.

Table 1
Cyclic voltammetric data[a] of ERG, TEL, HYQ and MEQ

| Substrate | Peak potential (V) | | | |
|---|---|---|---|---|
| | $E_{pc}$ | $E_{pa}$ | $\Delta E_p$ | $E_{1/2}$ |
| TEL | | | | |
| Wave I | −0.745 | −0.638 | 0.107 | −0.692 |
| HYQ | | | | |
| Wave I | −0.810 | −0.669 | 0.141 | −0.739 |
| Wave II | −1.358 | −1.226 | 0.132 | −1.292 |
| ERG | | | | |
| Wave I | −0.703 | – | – | – |
| Wave II | −0.908 | −0.743 | 0.165 | −0.826 |
| Wave III | −1.146 | −1.086 | 0.060 | −1.116 |
| MEQ | | | | |
| Wave I | −0.807 | −0.599 | 0.208 | −0.703 |
| Wave II | −1.117 | −0.831 | 0.286 | −0.974 |
| Wave III | −1.393 | −1.100 | 0.293 | −1.247 |

[a] Potentials in V against Ag/AgCl; scan rate: 100 mV/s.

### 3.4. Photocleavage of DNA by quinones

The photoactivated cleavage of covalently closed circular plasmid DNA by HYQ, MEQ and the reference compound, 1,4,5,8-tetrahydroxyanthraquinone (THQ), was studied in phosphate buffer (pH 7.4). In agarose gels, the electrophoretic mobility of DNA was followed. A typical electrophorogram, shown in Fig. 8, is a pictorial representation of the results obtained for experiments conducted for equal irradiation time with two different concentrations of HYQ and MEQ.

Lanes 1 and 2 are the dark and irradiated DNA respectively and these lanes serve as controls. Lanes 3 and 4 are the dark and irradiated solution of reference sample THQ with DNA. It is observed that the irradiated quinone THQ (0.1 mM) completely degraded the form I DNA. Lanes 5 and 6 represent the concentration-dependent photocleavage by HYQ. The intensity of form I is decreased for higher

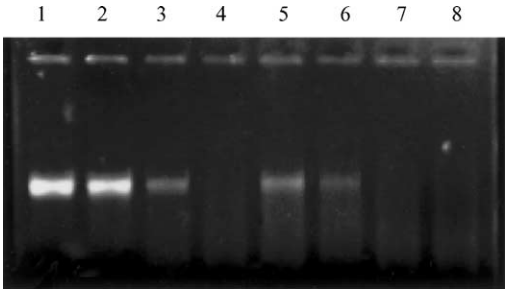


Fig. 8. Photoinduced cleavage of 3 μg plasmid DNA by HYQ and MEQ in phosphate buffer (pH 7.4) solutions. After 10 min irradiation, the loading dye was added and 20 μl aliquot of the solution was loaded into the gel. Lane 1: DNA (without irradiation); lane 2: DNA (with irradiation); lane 3: DNA + THQ (1 mM) (without irradiation); lane 4: DNA + THQ (2 mM); lane 5: DNA + HYQ (1 mM); lane 6: DNA + HYQ (2 mM); lane 7: DNA + MEQ (1 mM); lane 8: DNA + MEQ (2 mM).

concentration of HYQ. Similarly lanes 7 and 8 show the effect of concentration of MEQ on the DNA cleavage. In both the lanes, the form I is completely degraded. Thus a concentration-dependent DNA scission is observed for both HYQ and MEQ [31]. Comparison of lane 5 (HYQ) and lane 7 shows that MEQ exhibits greater photodamage. These observations correlate well with the higher $O_2^{\bullet -}$ generating efficiency of MEQ. Thus the role of ROS is well demonstrated in the in vitro photoactivated DNA scission [32]. Results of cytochrome *c* reduction assay also show good correlation between $O_2^{\bullet -}$ generation and DNA scission. Photoinduced DNA cleavage experiment was also carried out for ERG and TEL as similar to that of HYQ and MEQ. The observed results showed larger DNA strand break for TEL in accordance with its higher ROS generating efficiency (data not shown).

It is concluded that both electron transfer (Type I) and energy transfer (Type II) paths are involved in quinone photosensitisation. This conclusion has been reached by RNO bleaching, EPR-TEMPL method, SOD inhibitable cytochrome *c* reduction assay and DMPO spin trapping experiments. Based on the results reported above, the observed photoinduced cleavage of DNA is due to the ROS generating efficiency of the anthraquinones.

## Acknowledgements

Thanks are due to the UGC, New Delhi, for the award of a teacher fellowship and to the Managing Board, NMSSVN College, Madurai, Tamilnadu, for study leave to M.R. We thank the Department of Chemistry, Pondicherry University, Pondicherry, for providing EPR facilities. Financial assistance from UGC, New Delhi, to the School of Chemistry (Departmental Research Support) is gratefully acknowledged.

## References

[1] J.M. Bruce, Benzoquinones and related compounds, in: S. Coffey (Ed.), Rodd's Chemistry of Carbon Compounds, vol. III, part 4, 2nd ed., Elsevier, Amsterdam, 1974, pp. 1–306.
[2] A. Ashnager, J.M. Bruce, P.L. Dutton, R.C. Prince, Biochim. Biophys. Acta 801 (1984) 351.
[3] A.J. Carmichael, M.M. Mossoba, P. Reisz, FEBS Lett. 164 (1983) 401.
[4] K.J. Reszka, P. Bilski, C.F. Chignell, J.A. Hartley, N. Khan, R.L. Souhami, J. Mendonca, J.W. Lown, J. Photochem. Photobiol. 15 (1992) 317.
[5] J.J. Inbaraj, R. Gandhidasan, R. Murugesan, Photochem. Photobiol. A: Chem. 124 (1999) 95.
[6] M. Rajendran, S. Ramasamy, C. Rajamanickam, R. Gandhidasan, R. Murugesan, Biochim. Biophys. Acta 1622 (2003) 65.
[7] J.J. Inbaraj, M.C. Krishna, R. Gandhidasan, R. Murugesan, Biochim. Biophys. Acta 1472 (1999) 462.
[8] J.J. Inbaraj, R. Gandhidasan, R. Murugesan, Free Radic. Biol. Med. 26 (1999) 1072.
[9] B. Kalyananraman, C.C. Felix, R.C. Sealy, Photchem. Photobiol. 36 (1982) 5.
[10] I. Kraljic, S. El Mohsni, Photochem. Photobiol. 28 (1978) 577.
[11] E. Gandin, Y. Lion, A. Van De Vorst, Photochem. Photobiol. 37 (1983) 271.
[12] J. Johnson Inbaraj, R. Gandhidasan, R. Murugesan, J. Photochem. Photobiol. 124 (1999) 95.
[13] E. Gandin, Y. Lion, J. Photochem. Photobiol. 20 (1982) 77.
[14] P.C.C. Lee, A.J. Rodgers, J. Photochem. Photobiol. 45 (1987) 79.
[15] Y. Lion, M. Demelle, A. Van De Vorst, Nature 263 (1976) 442.
[16] J. Moan, E. Wold, Nature 279 (1979) 450.
[17] J.M. Mc Cord, I. Fridovich, J. Biol. Chem. 244 (1969) 6049.
[18] W.H. Koppenol, J. Butler, Isr. J. Chem. 24 (1984) 11.
[19] T. Maniatis, E.F. Fritsch, J. Sam brook, Molecular Coloning: A Laboratory Manual, Cold Spring Harbour Laboratory, Cold Spring Harbour, New York, 1984.
[20] C. Murali Krishna, S. Uppuluri, P. Riesz, J. Samuel Zigler Jr., D. Balasubramanian, Photochem. Photobiol. 54 (1991) 51.
[21] E. Wilkinson, J.G. Brummer, J. Phys. Chem. Ref. Data 10 (1981) 809.
[22] E.Ben. Hur, A. Carmichael, P. Riesz, I. Rosenthal, Int. J. Radiat. Biol. 48 (1985) 837.
[23] T. Ozawa, A. Hanaki, Chem. Pharm. Bull. 26 (1978) 2572.
[24] B. Kalyanaraman, C. Mottley, R.P. Mason, J. Biochem. Biophys. Methods 9 (1984) 27.
[25] R.A. Floyd, Biochim. Biophys. Acta 756 (1984) 204.
[26] G.R. Buettner, Free Radic. Biol. Med. 3 (1987) 259.
[27] B. Halliwell, J.M.C. Gutteridge, Free Radical in Biology and Medicine, 3rd ed., Oxford University Press, Oxford, 1999, p. 358.
[28] S.I. Dikalov, R.P. Mason, Free Radic. Biol. Med. 27 (1999) 864.
[29] R.J. Driebergen, J.J.M. Holthuis, A. Hulshoff, S.J. Postma-Kelder, W. Verboom, D.N. Reinhoudt, P. Lelieveld, Anticancer Res. 6 (1986) 605.
[30] G. Zagotto, S. Moro, E. Uriarte, E. Ferrazzi, G. Palu, M. Palumbo, Anti-Cancer Drug Design 12 (1997) 99.
[31] S.R. Chatterjee, S.J. Shetty, T.P.A. Devasagayam, T.S. Srivastava, Photochem. Photobiol. B: Biol. 41 (1997) 128.
[32] T. Koch, J. Dezz Ropp, S.G. Sligar, G.B. Schuster, Photochem. Photobiol. 58 (1993) 554.